

# GRB Remnants

Tsvi Piran and Shai Ayal

*Racah Institute for Physics, The Hebrew University, Jerusalem, Israel 91904*

## Abstract.

The realization that GRBs are narrowly beamed implied that the actual rate of GRBs is much larger than the observed one. There are 500 unobserved GRBs for each observed one. The lack of a clear trigger makes it hard to detect these unobserved GRBs as orphan afterglows. At late time, hundreds or thousands of years after a GRB, we expect to observe a GRB remnant (GRBR). These remnants could be distinguished from the more frequent SNRs using their different morphology. While SNRs are spherical, GRBRs that arise from a highly collimated flow, are expected to be initially nonspherical. We ask the question for how long can we identify a GRBR among the more common SNRs? Using SPH simulations we follow the evolution of a GRBR and calculate the image of the remnant produced by bremsstrahlung and by synchrotron emission. We find that the GRBR becomes spherical after  $\sim 3000\text{yr}(E_{51}/n)^{1/3}$  at  $R \sim 12\text{pc}(E_{51}/n)^{1/3}$ , where  $E_{51}$  is the initial energy in units of  $10^{51}\text{erg}$  and  $n$  is the surrounding ISM number density in  $\text{cm}^{-3}$ . We expect  $0.5(E_{51}/n)^{1/3}$  non-spherical GRBs per galaxy. Namely, we expect  $\sim 20$  non spherical GRBRs with angular sizes  $\sim \mu\text{arcsec}$  within a distance of 10Mpc. These results are modified if there is an underlying spherical supernova. In this case the GRBR will remain spherical only for  $\sim 150\text{yr}(E_{51}/n)^{1/3}$  and the number of non-spherical GRBRs is smaller by a factor of 10 and their size is smaller by a factor of 3.

## INTRODUCTION

A  $\gamma$ -ray burst (GRB) that originates within a galactic disk deposits  $\sim 10^{51}\text{ergs}$  into the ISM. This results in a blast wave whose initial phase produces the afterglow. The late phase of the blast wave evolution would result, as noted by Chevalier [1] in the context of supernova remnants (SNRs), in a cool expanding HI shell. The shell will remain distinct from its surrounding until it has slowed down to a velocity of  $\approx 10\text{kms}^{-1}$  [2], which should happen within  $2.3 \cdot 10^6\text{yr} E_{51}^{0.32}$  where  $E_{51}$  is the initial energy in units of  $10^{51}\text{erg}$ .

The observed rate of GRBs is one per  $\sim 10^7\text{yr}$  per galaxy [3]. The implied GRB isotropic energy is of the order of  $10^{53}\text{ergs}$ . These estimates suggested that there are a few remnants per galaxy at any given time. As it was believed that the GRB explosions were much more energetic than SNs, Loeb and Perna [2] suggested that GRBRs would form HI supershells. This giant structures require much more energy than what a usual SN can supply.

However, the realization that GRBs are beamed [4, 5, 6, 7, 8] changed both estimate. First the rate of GRBs is much higher. Beamed GRBs illuminate only a fraction  $f_b$  of the sky, thus their rate should be higher by a factor of  $f_b^{-1}$ . With  $f_b \sim 0.002$  [9] we expect several thousand

GRB remnants per galaxy. On the other hand the energy output of each GRB is much smaller [9, 10, 11]. Thus they cannot produce the giant HI shells.

How can we distinguish a GRBR from and SNR and for how long? Both GRBs and SNs deposit a comparable kinetic energy ( $\sim 10^{51}\text{erg}$ ) into the ISM. The energy injection in a GRB is in a form two narrow relativistic beams containing  $\sim 10^{-5}M_{\odot}$ . A SN deposits this energy spherically with  $\sim 10M_{\odot}$ . In both cases the expected late evolution is similar. At this late stage both remnants are in the Sedov [12] regime where all the kinetic energy is in the ejecta and all the mass is in the surrounding ISM. A key distinguishing feature unique to GRB remnants could be their beamed nature. We expect that the beamed emission would lead to a distinct double shell morphology at intermediate times. The late time behavior of the GRB remnant is expected to be spherical. To establish how many HI shells are GRB remnants we need to find out the expected morphology of GRB remnants and how long they stay non-spherical and distinguishable from SNRs. Establishing how many of the HI shells are GRB remnants would make it possible to directly estimate the local rate of GRBs, determine  $\epsilon$ , the efficiency of converting the explosion energy into  $\gamma$ -rays, and the beaming factor  $f_b$  [2].

We model the intermediate evolution of a beamed

GRB by two blobs of dense material moving into the ISM in opposite directions. We follow numerically the hydrodynamic evolution [13]. We find that the morphology depends on the dimensionless ratio between the accumulated mass and the initial kinetic energy,  $\mu \equiv Mc^2/E_0$ . When  $\mu \sim 2.1 \times 10^5$  (at  $t \sim 3000\text{yr}(E_{51}/n)^{1/3}$  and  $R \sim 12\text{pc}(E_{51}/n)^{1/3}$ ), the remnant becomes spherical and indistinguishable from a SNR.

An additional complication arises if the GRB is accompanied by a supernova, as suggested in the Collapsar model [14, 15, 16]. The supernova produces an underlying massive spherical Newtonian shell that propagates outwards. At  $\mu \sim 3000$  corresponding to  $t \sim 150\text{yr}(E_{51}/n)^{1/3}$  and  $R \sim 4\text{pc}(E_{51}/n)^{1/3}$  this shell will catch the non-spherical GRBR and the system will quickly become spherical. In this case the number of non-spherical GRBRs is smaller by a factor of 10 and their size is smaller by a factor of 3.

## THE NUMERICAL SIMULATIONS

### The Model

A GRB occurs when a compact ‘inner engine’ ejects two ultra-relativistic beams. Internal collisions within these beams leads to the GRB (See a schematic description in Fig. 1.). Later external shocks caused by collisions with circumstellar matter produce the afterglow. The matter slows down during this interaction and its bulk Lorentz factor  $\Gamma$ , decreases. The ejecta stays collimated only until  $\Gamma$  drops below  $\sim 1/\theta_0$ , at approximately  $2.9\text{hr}(E_{51}/n_1)^{1/3}(\theta_0/0.1)^{8/3}$  after the GRB [18, 4] where  $\theta_0$  is the initial angular width. At this time the matter starts expanding sideways causing, for an adiabatic evolution, an exponential slowing down [18]. The ejecta continues to expand sideways at an almost constant radial distance from the source  $R_0 \sim 0.3\text{pc} E_{51}^{1/3} n^{-1/3}$  until it becomes non-relativistic. At this stage, we begin our simulation.

Without a detailed numerical modeling of the relativistic phase of the ejecta we have only an approximate description of the initial conditions. We expect the angular width of the ejecta to be  $\sim 1$  rad and we are constrained by the energy conservation:

$$R_0 \sim 0.3\text{pc} E_{51}^{1/3} n^{-1/3} (v_0/c)^{-2/3}. \quad (1)$$

Our initial conditions comprise two identical blobs moving at  $v_0 \sim c/3$  in opposing directions into the ISM. Both the blobs and the ISM are modeled by a cold  $\gamma = 5/3$  ideal gas. The blobs are denser than the ISM.

Luckily the intermediate and late evolution of the ejecta are insensitive to the initial conditions. Already

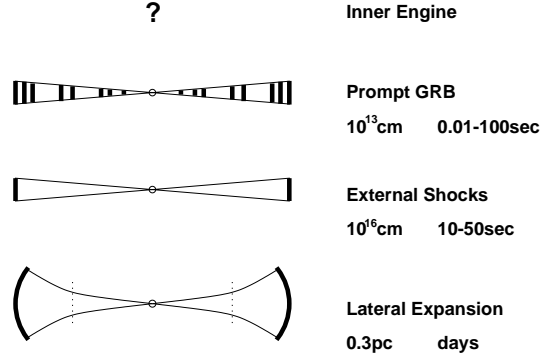


**FIGURE 1.** A schematic evolution of a GRB during its relativistic phase. From top to bottom: (a) An inner engine accelerates relativistic jets. (b) Collisions within the jets produce the observed GRB. (c) External shocks produce the afterglow. (d) The jets expand sideways as they slow down.

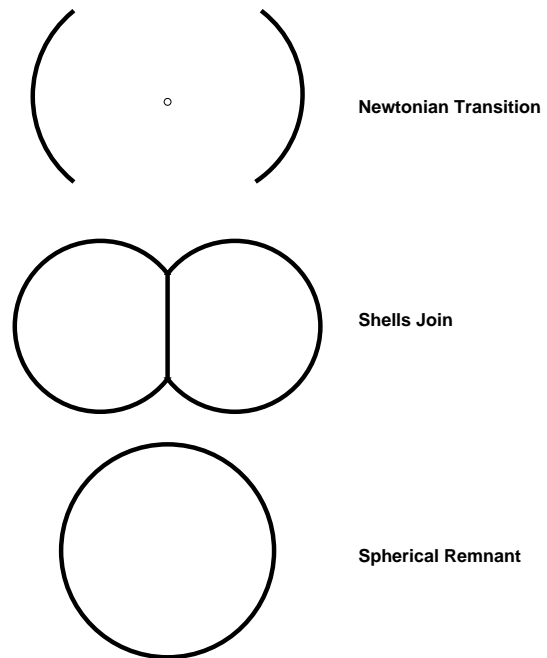


**FIGURE 2.** A schematic evolution of a GRBR. From top to bottom: (a) Initial conditions around the Newtonian transition. (b) Shells collision along the equatorial plane. (c) A late time spherical shell.

in the intermediate stage we are in the Sedov regime, the mass is dominated by the ‘external’ ISM gas which washes out any variations in the initial conditions of the ejecta. Our numerical simulations [13] verified this expectation and different initial densities, angular widths and shapes of the blobs led to essentially similar late time configurations.

Our code is based on the Newtonian version of the smooth particle hydrodynamics (SPH) code introduced

in [17]. The code was adapted for the specific problem at hand. We have also used the post Newtonian version of the code to take account of possible initial relativistic effects (with an initial blob velocity of  $c/3$ ).

Once we choose the initial velocity, Equation (1) leaves us with the freedom of choosing two out of the three parameters  $E_0$ ,  $R_0$  and  $n$ , the initial energy, distance and ISM density respectively. In presenting the results we choose  $E_0$  and  $n$ . To parameterize the evolution of the remnant we utilize the fact that mass scales linearly with initial energy and define the dimensionless parameter  $\mu = Mc^2/E_0$  where  $M$  is the accumulated shell mass. We define  $M$  as all mass with density above  $2n$ . We show all subsequent results as functions of  $\mu$ . The simulations begin with  $\mu \sim 1$ . Conveniently  $\mu$  scales linearly with time with:  $t \sim 0.046\mu(E_{51}/n)^{-1/3}$  yr, as can be seen from Fig. 3.

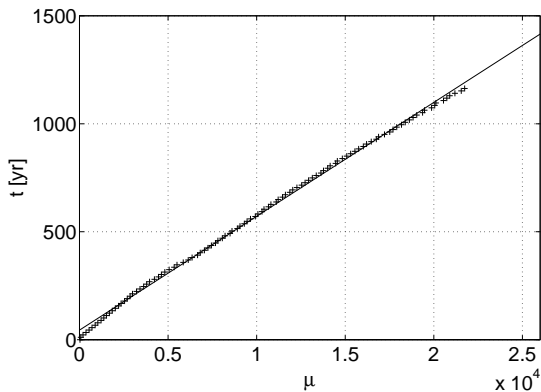


**FIGURE 3.** Time as a function of  $\mu$ . The linear relation between time and  $\mu$  is  $t \sim 0.046\mu(E_{51}/n)^{-1/3}$  yr.

## Results

As each blob collides with the ISM it produces a bow shock. This shock propagates also in the direction perpendicular to the blob's velocity. As the shocked blob material heats up it begins to expand backwards and a backwards going shock develops as well. The expected morphology of the remnant will therefore be of two expanding shells which will eventually join, producing yet another shock. At late times the shells merge and become a single spherical shell.

Fig. 2 depicts the expected schematic hydrodynamic behaviour after the Newtonian transition. This is indeed confirmed in the computation. Fig. 4, depicts the density contours along the evolution. We observe the expected evolution: from two individual blobs via a peanut shape configuration with a shock along the equator towards a more and more spherical configuration at late times.

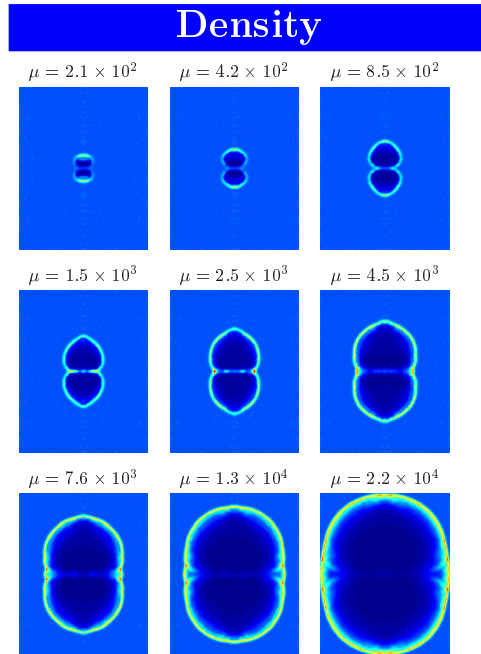


**FIGURE 4.** Equally spaced density contours ( $\rho = 1.5n, 2n, \dots, 3.5n$ ) at  $\mu = 9.5 \times 10^2, 1.4 \times 10^3, 2.4 \times 10^3, 3.9 \times 10^3, 6.1 \times 10^3, 10^4, 1.8 \times 10^4, 3 \times 10^4, 5 \times 10^4$  (left to right, top to bottom)

The ratio  $z_{\max}/r_{xy}$  can be approximated by a power law as shown in Fig 5. In our simulation this ratio is always between 1 and 2 so that the power law fit is very inaccurate. This ratio decreases in time as a power law with an exponent of  $-0.15$ . Extrapolating this power law we see that this ratio reaches a value of 1 at  $\mu \sim 2.1 \times 10^5$ . At this time the shock has a spherical shape with  $z = r_{xy} \sim 15(E_{51}/n)^{1/3}$  pc. Even then the shock will not be completely spherically symmetric as there would still be a ring of shocks around the “equator” where the shells have collided.

Figures 6 and 7 depict the images of the remnant as a function of time and angles of inclination. We show images due to bremsstrahlung emission and synchrotron emission. The images are constructed assuming that all the gas is optically thin in the relevant frequencies. The bremsstrahlung luminosity (Fig. 6) was calculated assuming that the volume emissivity is proportional to  $\rho^2 \epsilon^{1/2}$  [19]. In calculating the synchrotron emissivity (Fig. 7) we assumed that both the magnetic field energy density and the number density of the relativistic electrons are proportional to the internal energy density of the gas with constant proportionality factors  $\epsilon_B$  and  $\epsilon_e$

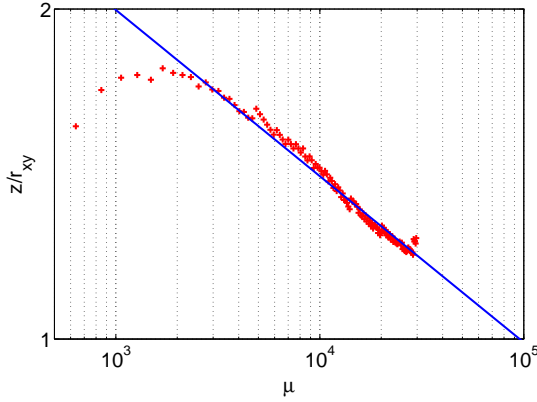


**FIGURE 5.** The ratio between the radius  $r_{xy}$  of the shock and the  $z$  position of the shock. The solid line is the best fit power law  $\mu^{-0.15}$ . The ratio will reach a value of 1 at  $\mu \sim 2.1 \times 10^5$  yr

respectively. We further assume that the relativistic electron number density is a power law in energy. Under these assumptions the volume emissivity is proportional to  $\rho^2 \epsilon^2$  [e.g. 20]. In the late images there are two bright circles at the lines where the colliding blobs form a hot shocked region. In figures 8 and 9 we show the characteristic emission frequencies. For bremsstrahlung this is  $kT/h$  where  $T$  is the temperature of the gas. For synchrotron emission we assume  $\epsilon_B = 0.1$ . The characteristic frequency in this case is the Larmor frequency  $eB/m_e$  where  $e$ ,  $B$  and  $m_e$  are the electron charge, the magnetic field and the electron mass respectively.

## DISCUSSION

The long time shape of a GRB remnant is insensitive to the exact initial morphology, angular width and density of the ejecta. Initially the remnant is highly non-spherical. It becomes spherical as time advances and the ratio between its height and radius approaches unity when

$$\mu \approx 2.1 \times 10^5. \quad (2)$$

This corresponds to

$$t \sim 10^4 \text{ yr } E_{51}^{1/3} n^{-1/3}, \quad (3)$$

and

$$R \sim 12 \text{ pc } (E_{51}/n)^{1/3}. \quad (4)$$

After this time it will be difficult to distinguish a GRB remnant from a SNR on the basis of its morphology alone.

Using as the observed GRB rate  $R_{GRB} = 10^{-7} \text{ yr}^{-1} \text{ gal}^{-1}$  [3] the expected number of non-

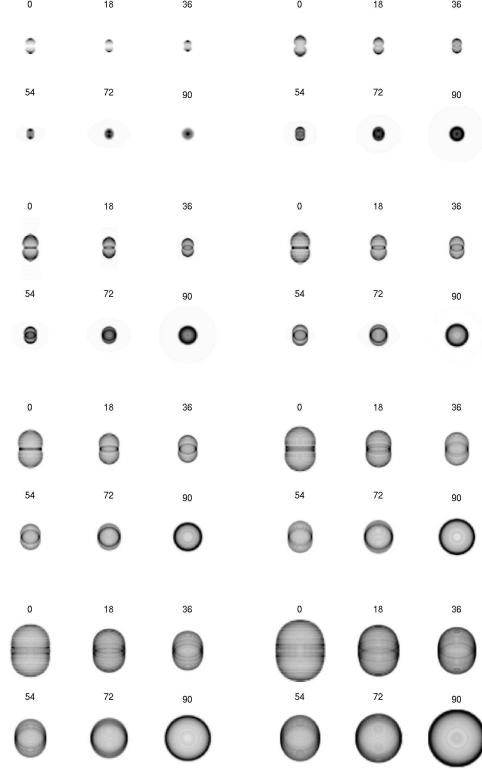


**FIGURE 6.** Images of the remnant, bremsstrahlung emission. The number above each image is the angle of inclination in degrees. The images are shown at the same  $\mu$  as the last 8 panels of figure 4.

spherical GRBRs per galaxy is:

$$0.5 \text{ yr}^{-1} \left(\frac{f_b}{500}\right)^{-1} \left(\frac{R_{GRB}}{10^{-7}}\right) E_{51}^{1/3} n^{-1/3}. \quad (5)$$

This value depends of course critically on the typical beaming factor,  $f_b$ . It should be compared with the expectation of 100 similar aged ( $10^4$  yrs) SNRs per galaxy. We would expect 20 non spherical GRBRs up to a distance of 10 Mpc. The angular sizes of these GRBRs would be around a  $\mu$ arcsec.

## Implications to DEM L 316

DEM L 316 [21] in the LMC looks like two colliding bubbles (see Fig. 10). It is thought to result from a collision between two SNRs. This requires, of course, an unlikely coincidence in the timing and the location of the two SNe. An interesting possibility is that DEM L 316 is a GRBR. Does this fit our model? DEM L 316 is far from spherical and has a distinct double shell morphology, most similar to our results at  $\mu \sim 10^4$

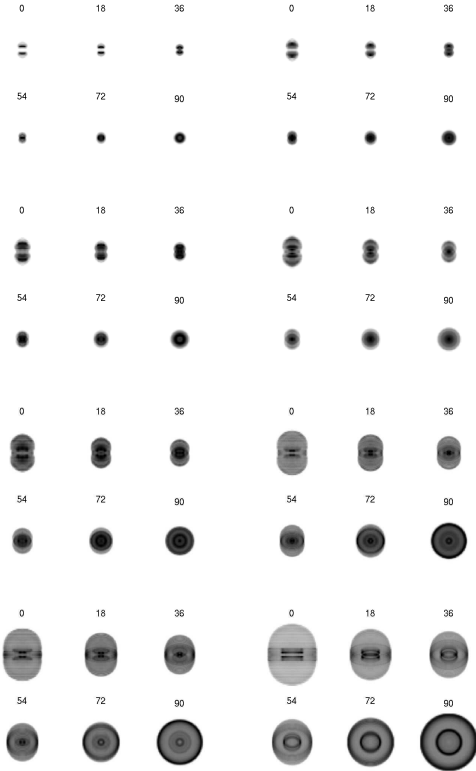


**FIGURE 7.** Images of the remnant, synchrotron emission. The  $\mu$  are the same as the last 8 panels in figure 6

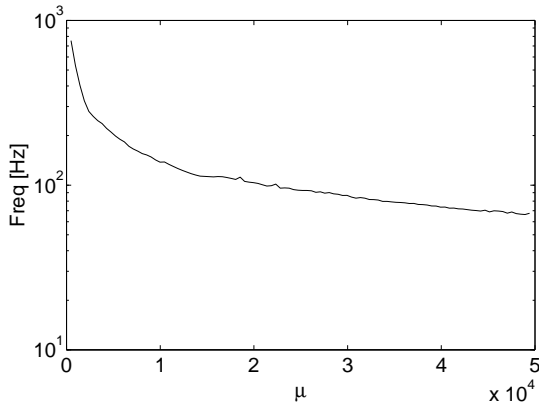


**FIGURE 8.** The characteristic synchrotron frequency as a function of  $\mu$ .

(see Fig. 4). The  $\mu$  ratio measured for DEM L 316 is  $\approx 7 \times 10^5$ . However, according to our results this is far after the spherical transition. A GRB remnant would already be spherical at this stage. This discrepancy rules out the possibility of fitting DEM L 316 with our model for a GRB remnant.

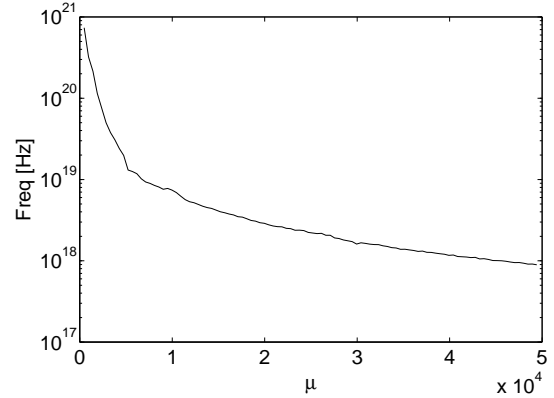


**FIGURE 9.** The characteristic bremsstrahlung frequency as a function of  $\mu$ .

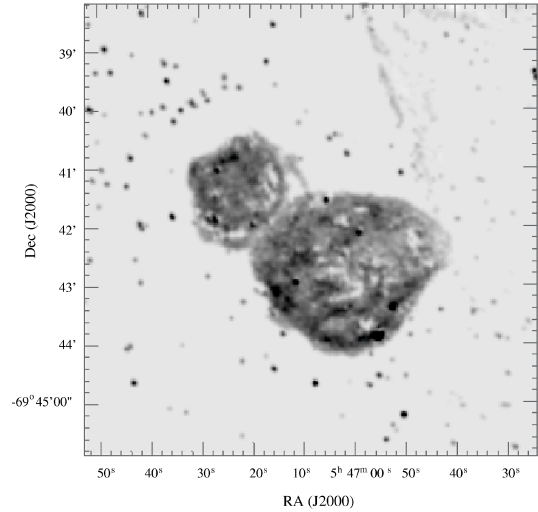


**FIGURE 10.** DEM L 316 in the LMC (from [21]).

## An Underlying Supernova

Our model should be modified if the GRB relativistic beams are accompanied by an underlying spherical supernova, as would be expected in the Collapsar model [14, 15, 16]. In this case a spherical shell of  $\sim 10m_{\odot}$ , the supernova ejecta, will accompany the GRB beams. This ejecta propagates at a much lower, Newtonian velocity, with initial values of  $\sim 10^4$  km/sec. However, it will not slow down while the outer GRB ejecta is piling up the external matter and is slowed down. Eventually it will catch the GRB ejecta. It is clear that at this stage the SN shell would tend to make the GRBR bow shock more spherical. To determine when this will happen one needs another set of numerical simulations. These are in progress now. However, we can attempt to estimate when the slower SN ejecta will catch up the slowing down

GRBR remnant. Assuming that the SN ejecta does not slow down (as the GRBR ejecta clears the surrounding ISM matter) we find that this will happen at:  $\mu \approx 3000$ , namely at  $t \approx 150\text{yr}(E_{51}/n)^{1/3}$  and  $R \approx 4\text{pc}(E_{51}/n)^{1/3}$ . This happens around the time that the two shells collide on the equator. We expect to see an enhanced emission due to this collision and then the system will become quickly spherical. The expected number of non spherical GRBRs and their corresponding sizes would be smaller by a factor of 10 than the values estimated earlier for the simple evolution of the beamed GRB ejecta. Thus we expect one or two non spherical GRBRs with distances up to 20 Mpc and their sizes would be around  $0.1 \mu\text{arcsec}$ .

## ACKNOWLEDGMENTS

This research was supported by a grant from the US-ISRAEL BSF.

## REFERENCES

1. Chevalier, R. A. 1974, Ap. J., 188, 501
2. Loeb, A. & Perna, R. 1998, Ap. J. Lett., 503, L35
3. Schmidt, M. 1999, Ap. J. Lett., 523, L117
4. Sari, R., Piran, T., & Halpern, J. P. 1999, Ap. J. Lett., 519, L17
5. Halpern, J. P., Kemp, J., Piran, T., & Bershad, M. A. 1999, Ap. J. Lett., 517, L105
6. Sari, R. 1999, in Proc. of the 5th Huntsville Gamma-Ray Burst Symposium
7. Kulkarni, S. R., Djorgovski, S. G., Odewahn, S. C., Bloom, J. S., Gal, R. R., Koresko, C. D., Harrison, F. A., Lubin, L. M., Armus, L., Sari, R., Illingworth, G. D., Kelson, D. D., Magee, D. K., van Dokkum, P. G., Frail, D. A., Mulchaey, J. S., Malkan, M. A., McClean, I. S., Teplitz, H. I., Koerner, D., Kirkpatrick, D., Kobayashi, N., Yadigaroglu, I., Halpern, J., Piran, T., Goodrich, R. W., Chaffee, F. H., Feroci, M., & Costa, E. 1999, Nature, 398, 389
8. Harrison, F. A., Bloom, J. S., Frail, D. A., Sari, R., Kulkarni, S. R., Djorgovski, S. G., Axelrod, T., Mould, J., Schmidt, B. P., Wieringa, M. H., Wark, R. M., Subrahmanyam, R., McConnell, D., McCarthy, P. J., Schaefer, B. E., McMahon, R. G., Markze, R. O., Firth, E., Soffitta, P., & Amati, L. 1999, Ap. J. Lett., 523, L121
9. Frail, D. A. and Kulkarni, S. R. and Sari, R. and Djorgovski, S. G. and Bloom, J. S. and Galama, T. J. and Reichart, D. E. and Berger, E. and Harrison, F. A. and Price, P. A. and Yost, S. A. and Diercks, A. and Goodrich, R. W. and Chaffee, F., 2001, Ap. J. Lett., 562, L55
10. Piran, T. and Kumar, P. and Panaitescu, A. and Piro, L., 2001, Ap. J. Lett., 560, L167.
11. Panaitescu, A. and Kumar, P., 2001, Ap. J. Lett., 560, L49
12. Sedov, L. I. 1959, Similarity and Dimensional Methods in Mechanics (New York: Academic Press)
13. Ayal, S. & Piran, T., 2001, Ap. J., 555, 23
14. S. E. Woosley, Ap. J., **405**, 273 (1993)
15. B. Paczynski, Ap. J. Lett., **494**, L45 (1998).
16. A. I. MacFadyen and S. E. Woosley, Ap. J., **524**, 262 1999, Ap. J., **524**, 262
17. Ayal, S. and Piran, T. and Oechslin, R. and Davies, M. B. and Rosswog, S., 2001, Ap. J., 550, 846
18. Rhoads, J. E. 1997, Ap. J. Lett., 487, L1
19. Lang, K. R. 1980, Astrophysical Formulae (Springer-Verlag)
20. Shu, F. H. 1991, The Physics of Astrophysics, Vol. 1 (University Science Books)
21. Williams, R. M., Chu, Y. H., Dickel, J. R., Beyer, R., Petre, R., Smith, R. C., & Milne, D. K. 1997, Ap. J., 480, 618